Removal of Selenocyanate in Water by Precipitation: Characterization of Copper−Selenium Precipitate by X-ray Diffraction, Infrared, and X-ray Absorption Spectroscopy

ARTICLE *in* ENVIRONMENTAL SCIENCE AND TECHNOLOGY · MARCH 1997

Impact Factor: 5.33 · DOI: 10.1021/es960138a

2 AUTHORS, INCLUDING:

Darrell L. Gallup
Chevron
66 PUBLICATIONS **477** CITATIONS

Environ. Sci. Technol. **1997**, *31*, 968−976

Removal of Selenocyanate in Water by Precipitation: Characterization of Copper−Selenium Precipitate by X-ray Diffraction, Infrared, and X-ray Absorption Spectroscopy

ALAIN MANCEAU*,† AND DARRELL L. GALLUP‡

Environmental Geochemistry Group, LGIT-IRIGM, University of Grenoble and CNRS, BP53, 38041 Grenoble Cedex 9, France, and Unocal Corporation, 1300 North Dutton Avenue, Santa Rosa, California 95401

During refining of sour crude oils produced from reservoirs containing seleniferous marine shales, selenium is concentrated into process waters and wastewaters. Selenium, present in the waters as selenocyanate, must be removed to meet regulatory discharge limits. Treatment of wastewaters with copper(II) salts effectively precipitates selenium. An objective of the present study was to determine whether selenium was precipitated as elemental Se or immobilized in the form of cyanate complexes or any other form that remains to be identified. The precipitate had a Se/(Se+S) mole ratio of 0.09. The incorporation of selenium in the copper thiocyanate lattice was proven by X-ray diffraction. The presence of native selenium was disallowed by Se K-edge X-ray absorption near-edge structure (XANES) and extended X-ray absorption fine structure (EXAFS) spectroscopy. Selenium was shown by EXAFS to be present as selenide and surrounded by one nearest C atom and three next-nearest Cu atoms. This local environment is typical of the copper thiocyanate structure, which proves that Se substitutes for S on the atomic scale. Based on results of chemical analyses and structural methods, it is concluded that the sludge consists primarily of an α-Cu($S_{0.91}Se_{0.09}$)CN solid solution. Some copper is not reduced and is liganded to O, OH, or H_2O. These results indicate that, when added to process water, cupric ions are reduced by sodium thiosulfate and sulfites initially present in the solution to yield primarily cuprous thiocyanate/selenocyanate.

Introduction

The remediation of water contaminated with selenium is often a difficult challenge due to the complex chemistry of the element. Waters in which selenium removal is especially complicated are found in the petroleum refining and mining industries. For example, sour crude oils produced from formations containing seleniferous marine shales often contain significant concentrations of selenium. Selenium is believed to be present in crude oil in the form of selenium analogs to sulfur-bearing species, such as mercaptans and thiophenes. As crude oil is processed to remove sulfur in refinery operations, selenium is removed as well in the form of hydrogen selenide, H_2Se, and other water-soluble selenium compounds (*1*). These process waters are typically disposed by direct discharge. Processing of certain mining ores may also result in contamination of surface and leach waters by selenium (*2*).

Although selenium is an essential trace nutrient, it is a poison at concentrations exceeding about 4 mg/kg (*3*). Toxic levels of selenium have contaminated both soils and waters in scattered locations across the world. To prevent human disease, the U.S. EPA has established a maximum contaminant level for selenium in drinking water of 0.05 mg/L (*4*). For environmental protection, treatment processes are required to remove selenium from agricultural, refinery, and mining wastewaters. Methods including adsorption, ion exchange, precipitation, reverse osmosis, etc. have been employed to remove selenium from drinking water and wastewater (*5*). The success of technologies for selenium removal is highly dependent on the initial selenium concentration and speciation (*6*). Speciation of selenium in certain petroleum refinery wastewater streams by a procedure using liquid chromatography with inductively-coupled plasma spectrophotometry/mass spectroscopy has detected the compound sodium selenocyanate, NaSeCN (*7*). Selenocyanates may also be present in mining wastewaters during cyanide leaching of selenide ores (*8*).

Ion exchange (*9*) and precipitation have been investigated as technologies to remove selenium (as selenocyanate) from refinery process and wastewater. Selenocyanate has been precipitated from aqueous solution upon reaction with gold, silver, cadmium, mercury, thallium, lead, and copper (*10, 11*). However, the precipitates have not been well-characterized. In addition to these sparingly soluble compounds, selenocyanates may form a variety of complexes with several transition metals (*12*). Unfortunately, most of metals that effectively precipitate selenocyanate from aqueous solution are generally regulated in the same way as discharges of selenium. Treatment of water with the majority of these metals is also prohibitively expensive. Among them, copper is the least toxic and most inexpensive to precipitate selenocyanate from waters, and it may be post-precipitated to below regulatory standards with sulfide (as covellite, CuS).

A petroleum refinery process water containing approximately 6 mg/L selenocyanate, $SeCN^-$, was utilized in our investigations of selenocyanate precipitation. The addition of silver(I), tin(II), gold(I), and copper(II) to this water formed precipitates and significantly decreased the selenocyanate ion concentration. By contrast, iron(II), iron(III), manganese(II), nickel(II), zinc(II), and tin(IV) had little effect on selenocyanate concentration. Treatment of this water with excess copper(II) salts to remove selenocyanate appears feasible and attractive for this application due to efficacy and low cost, although some of the copper appears to complex with carboxylic acids present in the process water. Furthermore, the U.S. EPA drinking water action limit is relatively high (1.3 mg/L). The precipitate resulting from copper(II) salt addition to the refinery process water consisted primarily of a poorly crystalline copper-rich material, X-ray diffraction detecting compounds resembling copper thiocyanates. The purpose of the present study is 3-fold: (i) to identify the mineralogical nature of the copper−selenium sludge precipitated by this process, (ii) to determine the structural form of selenium, and (iii) to propose a chemical reaction scheme for this selenium removal process.

Materials and Methods

Sample Description. A wastewater (pH 9.6) containing 7 mg/L selenocyanate ($SeCN^-$), 65 mg/L chloride, 15 mg/L

* Corresponding author fax: 33 4 76 51 44 22; e-mail: manceau@lgit.observ-gr.fr.
† University of Grenoble and CNRS.
‡ Unocal Corporation.

S0013-936X(96)00138-1 CCC: $14.00

thiocyanate, 165 mg/L thiosulfate, 5 mg/L sulfite, and 15 mg/L sulfate was treated with 2 g/L cupric chloride dihydrate, $CuCl_2 \cdot 2H_2O$. The selenocyanate concentration in the water was reduced to <0.1 mg/L upon rapid precipitation of a brown solid. The sludge precipitate was filtered, washed with water, and dried for 18 h at 100 °C. The concentrations of Cu, S, and Se were determined by X-ray fluorescence with an accuracy of ±0.1 wt %. These concentrations are equal to 39.0, 11.4, and 2.7 wt %, respectively. The high amount of copper in the sludge (Cu/(S+Se) = 1.6) results from the addition in excess of copper chloride to remove selenium as completely as possible.

Three reference samples were also synthesized: copper selenocyanate, CuSeCN, prepared by adding 0.1 mol of sodium thiosulfate to a solution mixture containing 0.1 mol each of cupric sulfate and potassium selenocyanate (*11*); a white copper thiocyanate, CuSCN, obtained by adding a 20% mol excess of sulfurous acid to a solution mixture containing 0.1 mol each of cupric sulfate and potassium thiocyanate; and a mixed copper thioselenocyanate precipitate, $CuS_{0.95}Se_{0.05}CN$, prepared by adding 0.1 mol of sodium thiosulfate to a solution mixture containing 0.1 mol of cupric sulfate, 0.01 mol of KSeCN, and 0.09 mol of KSCN. These three references have Cu/(S+Se) ratios of 1.5, 0.9, and 1.0, respectively. The high value for CuSeCN (1.5) suggests the presence of a copper-bearing impurity.

Samples Analysis. Infrared spectroscopy (IR) was performed on an ATI/Mattson Research FT-IR spectrometer (resolution 5 cm^{-1}). Spectra were recorded in transmission mode on pellets in a KBr matrix. Powder X-ray diffraction (XRD) patterns were recorded on a Siemens D5000 diffractometer equipped with a Si/Li solid detector. This solid detector has low intrinsic noise compared to classical detectors such as proportional counters, thus allowing improvement of the signal to noise ratio for XRD patterns. Cu Kα radiation was used with a counting time of 20 s per 0.03° 2θ step. The absolute precision of Bragg angles was determined with quartz and was found to be better than 0.01°/2θ on the full angular range. Unit-cell edge lengths were calculated after removing the contribution of the Cu $K\alpha_2$ radiation.

Cu and Se K-edge X-ray absorption near-edge structure (XANES) and extended X-ray absorption fine structure (EXAFS) spectra were collected at ambient temperature and in transmission mode on the EXAFS I station at the LURE synchrotron facility at Orsay, France. The positron storage ring operated at 1.85 GeV with an average beam current of ~300 mA. A Si(331) channel-cut monochromator was used. Gas ionization chambers were filled with an argon/helium mixture to attenuate the beam intensity by ≈20% before and ≈50% after the samples. The reproducibility in energy for XANES spectra was better than 0.1 eV.

Explanations of the XANES and EXAFS techniques are not attempted here; readers in search of theoretical details or applications to materials science and mineralogy or data reduction procedures are referred to recent books or general reviews on this subject (*13*−*16*). Fourier transforms were performed by using a Kaiser windowing function to minimize the intensity of side-lobes (*17*, *18*). Interatomic distances and the number of atoms in the two first Cu and Se coordination shells were determined by least squares inverse Fourier transform with theoretical phase shift and amplitude functions (*19*). Amplitude calibration and threshold energy adjustment (ΔE_0) were made with β-CuSCN, α-CuSeCN, and CuO as references. From the comparison between EXAFS and crystallographic data, precision on interatomic distances and on the number of atoms was estimated to be ±0.03 Å and ±30%.

TABLE 1. Infrared Wavenumber for C−N Stretching Mode in Various Thiocyanate and Selenocyanate Compounds[a]

	wavenumber (cm^{-1})
reference	
Ct−N−C−Se	2050−2090
Ct−Se−C−N	2070−2130
Ct−Se−C−N−Ct	>2100
K−S−C−N	2068
K−Se−C−N	2070−2078
α-CuSCN	2157
β-CuSCN	2173
sample	
β-CuSCN	2174
α-CuSeCN	2157
$CuS_{0.95}Se_{0.05}CN$	2161 + 2176
sludge	2161

[a] After refs 20, 21, 31, and 32. Ct, transition metal.

Results

IR. Thiocyanate (SCN^-) and selenocyanate ($SeCN^-$) ions may coordinate with transition metal ions through N and/or S,Se ligands. These three ways in which the $(S,Se)CN^-$ group may bond copper can be schematized as follows: Cu−N−C−(S,Se), Cu−(S,Se)−C−N, and Cu−(S,Se)−C−N−Cu (*20*). The CN stretching frequency has been shown to be characteristic of the type of bonding and may serve as a useful guide in differentiating these three types of coordination complexes. Table 1 shows that the CN stretching mode increases from 2050−2090 to 2070−2130 cm^{-1} and to >2100 cm^{-1} in structures I, II, and III, respectively. For all samples, a sharp band comprised between 2156 and 2176 cm^{-1} was observed, suggesting the type of coordination to be Cu−(S,Se)−C−N−Cu. CuSCN has a band at 2174 cm^{-1} and CuSeCN has a band at 2157 cm^{-1}, which correspond to those reported for β-CuSCN (2173 cm^{-1}) and α-CuSCN (2157 cm^{-1}) (*21*). One may thus conclude that the thiocyanate sample crystallized in the β polymorphic form, and the selenocyanate sample crystallized in the α form. This interpretation assumes that the CN stretching mode is not markedly modified by the Se for S substitution, but support is provided by the comparison of stretching modes in KSCN and KSeCN (Table 1). The mixed $CuS_{0.95}Se_{0.05}CN$ cyanate sample has a double CN peak at 2161 and 2176 cm^{-1}, which suggests a mixture of the α and β forms, whereas the sludge sample displays a single sharp maximum at 2161 cm^{-1} assigned to the α form.

XRD. Results of XRD analysis are presented in Figure 1 and Table S1 in the Supporting Information. XRD patterns for CuSCN confirm that this sample crystallized in the β form. Trace impurity of the α polymorph was detected. All lines of the sludge precipitate and of CuSeCN could be indexed with the α-CuSCN structure; no other phases were identified. Examination of Figure 1 shows that 002 and 012 lines for $CuS_{0.95}Se_{0.05}CN$ are not resolved, with a broad feature observed between 26° and 29° 2θ. This broadening is interpreted by the presence of β-Cu(S,Se)CN impurity because the intense 101 line of this component peak in-between the 002 and 012 lines of the α-Cu(S,Se)CN component. As noted in Figure 1, the presence of this β form causes several lines of the α compound to be asymmetric or broadened. However, in this diffraction pattern, reflections from the α form clearly dominate over those of the β form, and the former polymorph is thus believed to be more abundant than the second. These XRD results are in fair accord with infrared data and suggest that cupric ions were reduced to the cuprous state to form selenothiocyanate complexes. Specifically, the absence of XRD lines at 14.90°, 17.40°, and 20.78° 2θ allows us to assume a lack of copper(II) cyanate $Cu((S,Se)CN)_2$ complexes in these samples.

XRD lines for the three Se-containing samples were found to be shifted to lower angles relative to pure α-CuSCN. This

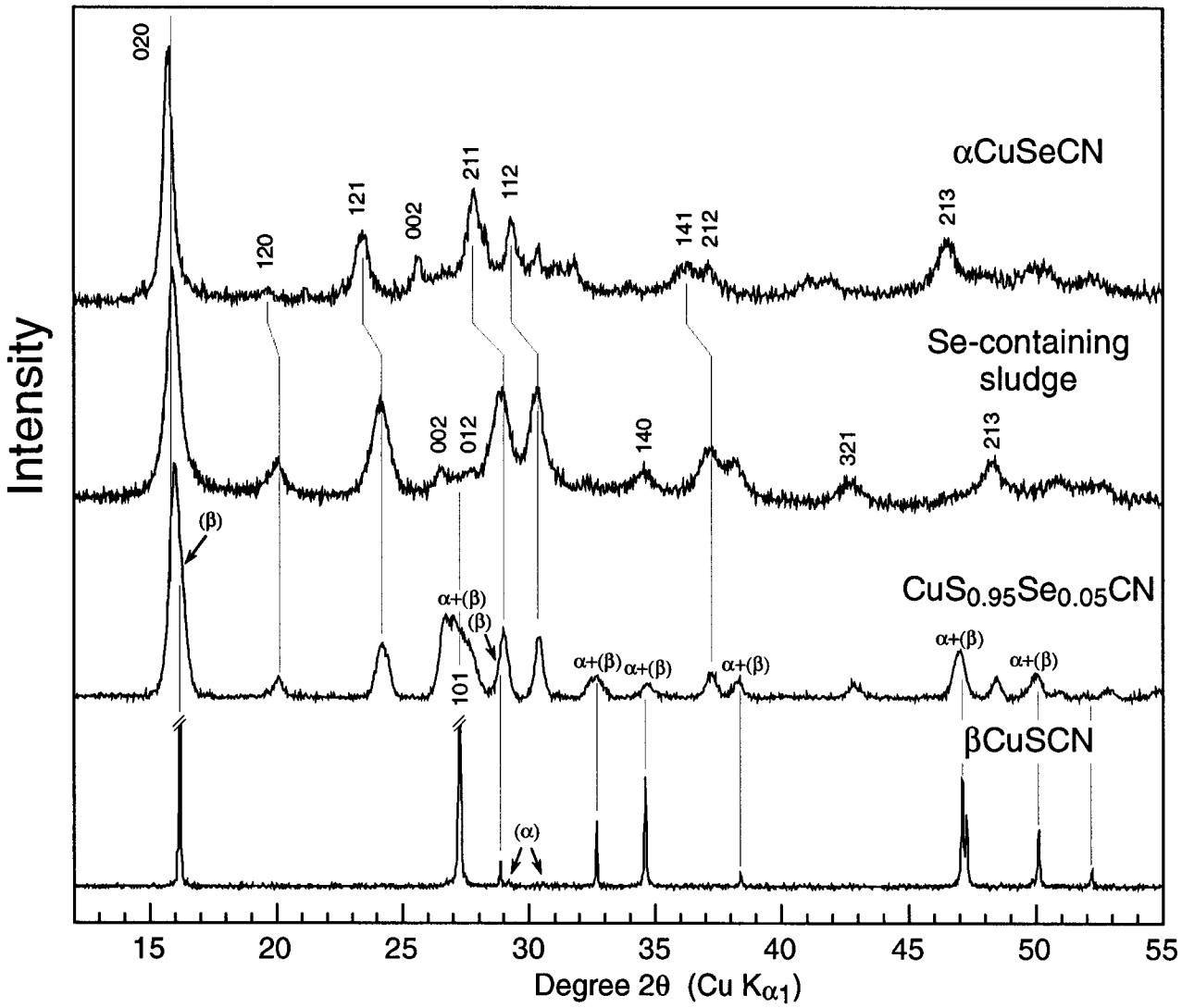

FIGURE 1. Comparison of XRD patterns for the references and the sludge sample.

shift is caused by the greater size of Se^{2-} anion (1.98 Å) as compared to S^{2-} (1.84 Å) (*22*). Unit-cell edge lengths were calculated by a least squares fitting procedure using 7−9 *hkl* reflections (Figure 2). Despite the relatively low number and width of X-ray lines used for this determination, the standard deviation on *a*, *b*, and *c* was typically 0.01 Å, which is fair in regard to the variation range between the two end members: $\Delta a = 0.37$ Å, $\Delta b = 0.2$ Å, and $\Delta c = 0.27$ Å (Figure 2 and Table S1 in the Supporting Information). Se^{2-} is larger than S^{2-} by 8%, and the size of the unit-cell for α-CuSeCN is greater than that of α-CuSCN by only 2−5%. A parallel can be made with the α-FeOOH−α-AlOOH solid solution where the differences between Al and Fe ionic radii is 16% while the difference in unit cells parameters is 5−6%. Figure 2 shows that unit-cell parameters for the α component of $CuS_{0.95}Se_{0.05}CN$ and the sludge samples are greater than those of αCuSCN and, to the precision of the measurement, follow Vegard's law (*23*). Accordingly, the greater the Se content, the greater the unit-cell parameters, reflecting the increasing Se for S substitution in thiocyanate frameworks. Note in Figure 1 that the shift to lower angles is accompanied by minor peak intensity differences. Structure factors of *hkl* reflections are thus modified by the presence of selenium in the various solids, and this observation adds strength to the previous conclusion about the isomorphous nature of Se for S substitution.

XANES. This technique examines the variation of the absorption of X-rays with wavelength in the vicinity of an absorption edge. At the K-edge a core level 1s electron is ejected toward external empty states. A positive energy shift of several electronvolts in the absorption threshold follows an increase in the formal valence of the element, allowing its valence to be determined in unknown compounds (*15, 24*). XANES spectra and their derivatives for the references and sample are presented in Figure 3. As a first approximation, one may consider that the energy position from the sludge sample is similar to that of the reference, indicating a reduction of Cu from the cupric to the cuprous oxidation state following the copper addition to the wastewater. However, a closer look at Figure 3a indicates that the sludge edge spectrum is slightly shifted to higher energy by ≈0.4 eV, which suggests the possible presence of some unreduced cupric ions. A comparison of Se-XANES spectra allows us to conclude that selenium is present as selenide anions (Figure 3b). The edge crest of the XANES spectrum for elemental selenium is shifted to lower energy by as much as 5 eV relative to selenide compounds. Based on the importance of this chemical shift, an energy reproductibility of 0.1eV, and a shift threshold of 0.4eV needed for a clear assignment, the maximum amount of Se^0 in this sample is estimated to be 10%, if any.

Absorption features observed in the steeply rising part of the Cu K-edge spectra can be ascribed to transitions to tightly bound, unfilled, molecular orbital (MO) levels (*24*). Their energy and intensity are determined by dipolar rules and reflect the unoccupied density of states of p-like character (1s − np transitions with $n = 4$ for Cu K-edge). Spectral features in this energy range are thus influenced by the

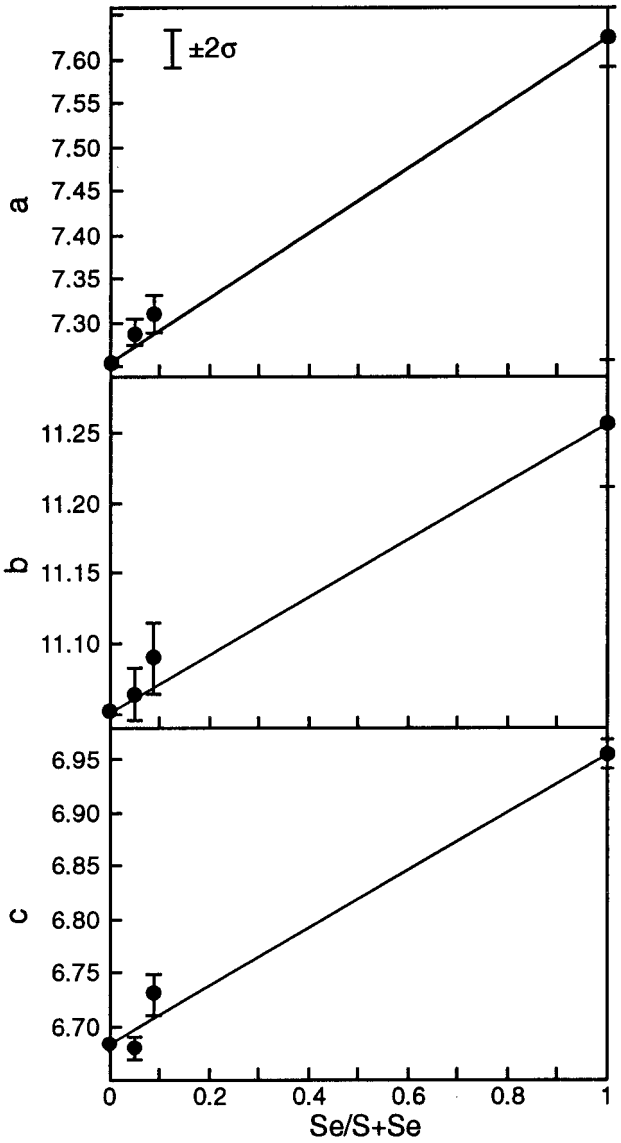

FIGURE 2. Unit-cell parameters for α-CuSCN, $CuS_{0.95}Se_{0.05}CN$, the sludge, and α-CuSeCN as a function of the Se/(Se+S) mole fraction. Se/(Se+S) are equal to 0.0, 0.05, 0.09, and 1.0, respectively. Parameters for α-CuSCN are from the JCPDS card 29-582. α polymorphs have an orthogonal unit cell with $a = 7.62$ Å ($\sigma = 0.02$ Å), $b = 11.26$ Å ($\sigma = 0.02$ Å), $c = 6.95_6$ Å ($\sigma = 0.007$ Å) for α-CuSeCN, $a = 7.28_7$ Å ($\sigma = 0.008$ Å), $b = 11.06$ Å ($\sigma = 0.01$ Å), $c = 6.68_0$ Å ($\sigma = 0.005$ Å) for $CuS_{0.95}Se_{0.05}CN$, and $a = 7.31$ Å ($\sigma = 0.01$ Å), $b = 11.09$ Å ($\sigma = 0.01$ Å), $c = 6.73$ Å ($\sigma = 0.01$ Å) for the sludge. Crystallographic data are tabulated in Supporting Information.

structure and chemical nature of the first ligand sphere surrounding the metal site, and as one might expect, similar crystalline structures result in similar spectra, both in the position and amplitude of features. Figure 3a shows that the XANES spectrum for the sludge sample is relatively featureless in comparison with the others: the two prominent maxima at 8972 and 8978 eV (arrows) are broadened, and their intensity is lowered. This observation points to a difference of the electronic structure of copper in this sample and, hence, to some differences in its crystal chemistry as compared to pure copper(I) cyanate reference compounds. Since the chemical analysis indicated that copper was in excess by approximatively 60% with respect to the stoichiometry of copper thiocyanate (Cu/(S+Se) = 1.6), one may conclude that the spectral shift and the broadening of this sludge sample are likely a result of the presence of poorly crystallized Cu^{2+}-containing impurities not detected by XRD. It will be shown below that this inference is also supported by EXAFS data.

EXAFS. This spectroscopy was used to complement IR, X-ray diffraction, and XANES to get deeper insight into the crystal chemistry of copper and selenium in the references and sample. In contrast to IR and XRD, EXAFS is chemically selective and is sensitive to the local structural environment of a selected atom, i.e., Cu and Se in the present study (*15, 16*).

Cu K-edge. Cu K-edge radial distribution function (RDF) peaks obtained by a Fourier tranformation of normalized EXAFS spectra are contrasted in Figure 4a. Several peaks are observed below ~5 Å, which correspond to the contribution of nearest atomic shells surrounding Cu atoms. RDF peaks are shifted to shorter distances relative to crystallographic values by approximately 0.3−0.5 Å because no correction for phase shift functions was attempted at this stage of the data analysis (*13*). Based on crystallographic data (Table S2 in the Supporting Information), first RDF peaks at the apparent distance of ~1.5 Å are assigned to Cu−N pairs, the second at ~2 Å to Cu−(S,Se) pairs, and the third at ~2.8 Å to Cu−C pairs. The nature of atoms in the various coordination shells at increasing distance is in agreement with the chain Cu−(S,Se)−C−N−Cu structure of these copper(I) selenothiocyanate complexes determined by IR. For steric reasons, the Cu−Se peak for α-CuSeCN is shifted to longer distance relative to Cu−S for β-CuSCN. The shape of the RDF for the sludge sample is specific. Its first peak has a higher amplitude and is shifted to higher energy as compared to the references, its second peak is lower, and the third peak is practically absent.

Structural parameters derived by least squares fitting of the contribution to EXAFS of the first two atomic shells (N, S/Se) are reported in Table 2. Cu−N and Cu−S distances obtained with theoretical phase shift functions of McKale (*19*) for the reference β-CuSCN are shorter than crystallographic values by 0.02−0.03 Å, which is fairly acceptable. Good spectral fits of the two first RDF peaks for $CuS_{0.95}Se_{0.05}$-CN and α-CuSeCN were obtained by assuming N and S/Se nearest and next-nearest neighbors at distances of 1.91 and 2.31−2.41 Å. These values are characteristic of copper(I) cyanate structures as in copper(II) dithiocyanate structures ($Cu(SCN)_2$), Cu−N and Cu−S distances are equal to ~2.00 and ~3.00 Å, respectively (*25, 26*). Note however that the number of Se neighbors (N_{Cu-Se}) in α-CuSeCN is equal to ~2.0, which is a little lower than the expected value of 3. This result suggests that the speciation of copper in this sample may not be as unique as previously inferred from the chemical analysis (Cu/(S+Se) = 1.5). Attemps to detect the presence of Se atoms in the second coordination shell of Cu in $CuS_{0.95}$-$Se_{0.05}CN$ failed as a result of the relatively low amount of selenium in the structure.

The salient result of this Cu K-edge study comes from the analysis of the sludge sample. For this sample $R_{Cu-(N,O)} = 1.95$ Å and $N_{(N,O)} = 2.2$ (Table 2). These values are too high to fit with a pure cyanate structure and clearly point to the presence of other chemical form(s). This distance of 1.95 Å is typical of cupric ion coordinated to oxygen, and similar structural results (i.e., *R* and *N*) were obtained by assuming either N or O as nearest neighbors since these two elements are too close in the classification to be discriminated by EXAFS (*16*). The inference of cupric rather than cuprous ions liganded to oxygen can be substantiated by comparing nearest Cu−O distances in CuO and Cu_2O, which are equal to 1.95−1.96 and 1.84 Å, respectively (*27, 28*). In general, Cu−O distances are much shorter in Cu^+ structures than in Cu^{2+} structures because cuprous ions are usually 2- or 4-fold coordinated and thus possess a smaller ionic radii (0.46 or 0.60 Å) than cupric ions, which are generally 6-fold coordinated (0.73 Å) (*22*). Based on these crystal chemical considerations, the distance of 1.95 Å determined in the sludge sample can be interpreted by the presence of Cu^{2+}−(O,OH, OH_2) pairs. The mineralogical nature of this Cu-bearing phase remains unknown, but due to the chemical composition of

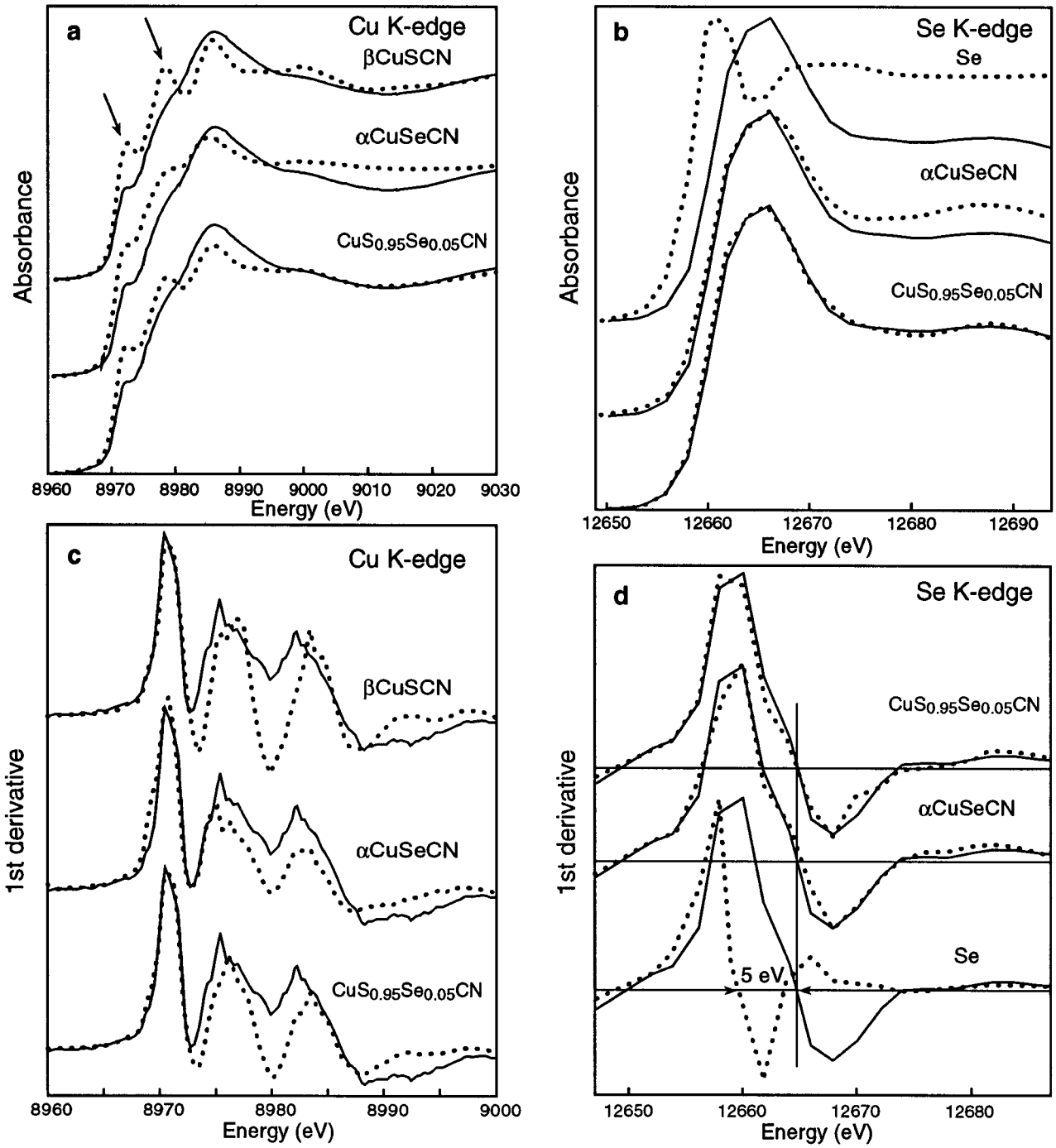

FIGURE 3. XANES spectra (a, b) and first derivatives (c, d) for reference compounds (dotted lines) and the sludge (solid line). (a and c) Cu K-edge; (b and d) Se K-edge.

the sludge, this phase is believed to be a copper oxyhydroxide or salt. This impurity is certainly poorly crystallized as it is not detected by XRD. The presence of copper(I) thiocyanate in this sample, as determined by XRD, is however confirmed by the presence of S next-nearest neigbors at 2.30 Å (Table 2).

The mixture of a cupric and cuprous phase in this sample is also consistent with the amplitude analysis of Cu−N, Cu−O, and Cu−S EXAFS contributions. In the sludge, the number of nearest oxygens (N_O = 2.1) is found to be significantly lower than the value of 4 expected in a pure cupric oxide and salt structure and higher than that expected in a pure cyanate structure (N_N = 1). Likewise, N_S = 1 instead of 3 in the absence of cupric impurity (Table 2). The drop in amplitude of the Cu−S peak for the sludge sample stems from this phase mixture since cupric oxide and salt structures have no atomic shells at ~2.3 Å. More generally, this assumption of a cupric and cuprous phase offers a clue to the peculiar shape of the sludge RDF. This is examplified in Figure 4b, which compares the imaginary parts and the modulus of the Fourier transforms for the sludge, $CuS_{0.95}Se_{0.05}CN$, and CuO between 1.4 and 2.2 Å. As seen in this figure, the shape of the modulus and imaginary part of the sludge RDF can precisely be reproduced by combining the imaginary parts of $CuS_{0.95}Se_{0.05}CN$ and CuO RDFs. For instance, the minimum in the RDF modulus for the sludge observed at 1.85 Å (third vertical line) can be explained by the fact that the imaginary parts of $CuS_{0.95}Se_{0.05}$-CN and CuO are out of phase. Likewise, the intermediate amplitude of the sludge RDF at 1.65 and 2.05 Å relative to $CuS_{0.95}Se_{0.05}CN$ and CuO (second and third vertical lines) is fully accounted by the intermediate intensity of its imaginary part as compared to the cupric and cuprous references. This

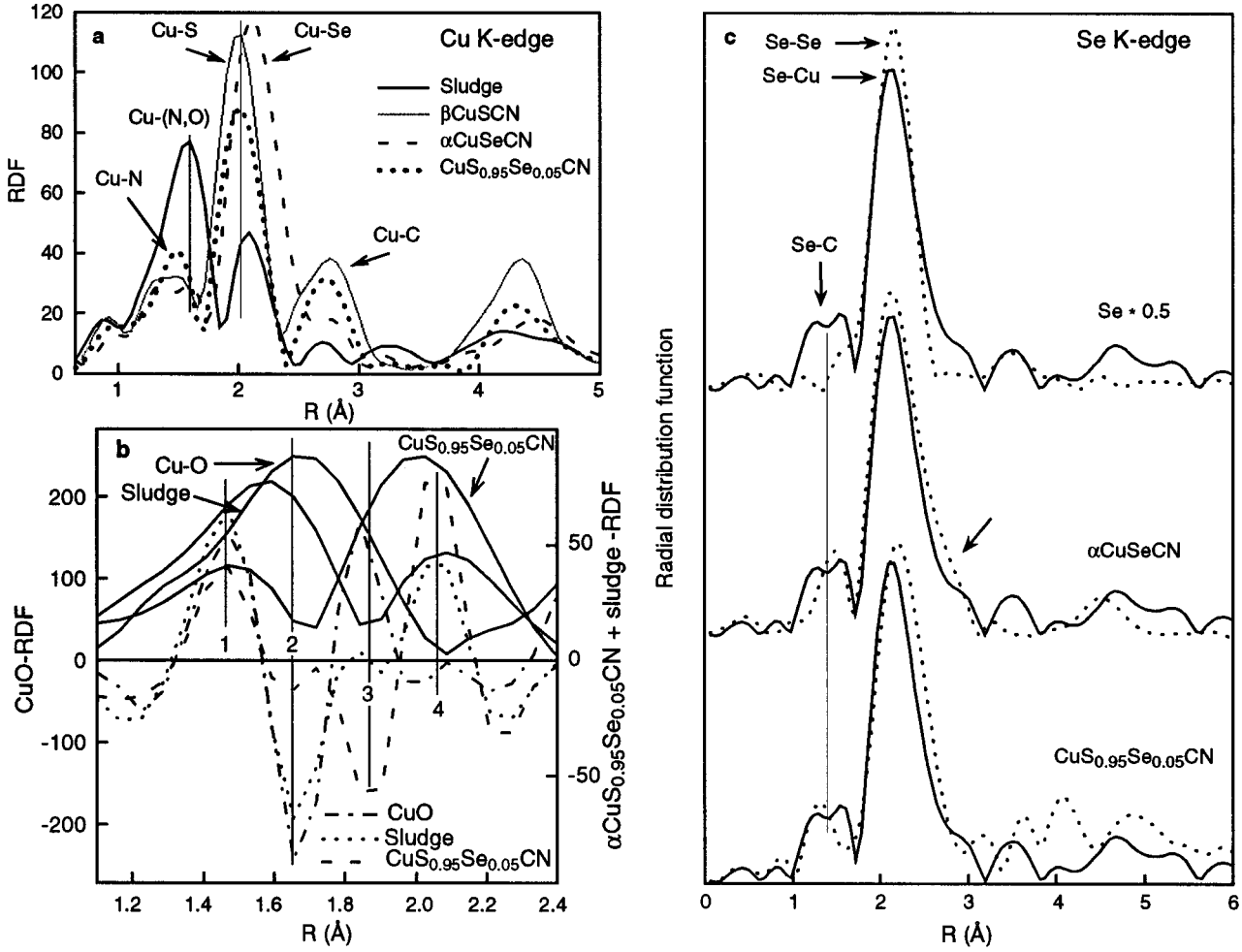

FIGURE 4. (a) Comparison of Cu K-RDFs for the references and the sludge sample. These functions correspond to the modulus of the complex Fourier transform ± $(Re^2 + Im^2)^{1/2}$. (b) Modulus (envelope curves) and imaginary part (oscillatory curves) of the Fourier transform for the references and the sample. Since RDFs are not corrected for phase shift functions, their peaks are shifted toward shorter distances by ~0.3−0.5 Å with respect to crystallographic values. (c) Comparison of Se K-RDFs for the references (dotted lines) and the sludge sample (solid line). Interatomic distances in copper(I) thiocyanates references (α/β-CuSCN) are reported as Table S2 in the Supporting Information.

TABLE 2. EXAFS Structural Parameters for References and Sample[a]

K-edge	sample	atomic shell	*R* (Å)	*N*	*σ* (Å)	Δ*E* (eV)	*Q*
Cu	β-CuSCN	N	1.91	1.0	0.09	0^+	0.02
		S	2.31	3.0	0.11	0^+	
Cu	$CuS_{0.95}Se_{0.05}CN$	N	1.91	0.6	0.07	-2^+	0.01
		S	2.31	2.5	0.11	-2^+	
Cu	α-CuSeCN	N	1.91	0.6	0.08	0*	0.02
		Se	2.41	2.0	0.10	9	
Cu	sludge	O	1.95	2.1	0.10	−10*	0.01
		S	2.30	1.0	0.13	1	
Cu	CuO	O	1.96	4.0	0.07	−10	0.005
Se	α-CuSeCN	C	1.85	1.0	0.08	−15*	0.05
		Cu	2.39	2.4	0.06	-7^+	
		Cu	2.52	0.6	0.02	-7^+	
Se	$CuS_{0.95}Se_{0.05}CN$	C	1.80	1.3	0.13	−15*	0.05
		Cu	2.40	1.9	0.07	-9^+	
		Cu	2.51	0.6	0.00	-9^+	
Se	sludge	C	1.69	0.3	0.00	−15*	0.06
		C	1.86	0.9	0.04	−15*	
		Cu	2.42	3.0	0.09	−7*	

[a] Δ*E*, deviation from the threshold energy taken at Δμ/2. *Q*, figure of merit for the spectral fitting. $Q = \Sigma(k^3\chi_{exp} - k^3\chi_{th})^2/\Sigma(k^3\chi_{exp})^2$. (+) value allowed to vary during the fitting but held identical for the two shells. (*) Parameter fixed during the fitting. *R* window for copper cyanates, 1.0−2.4 Å; for Se, 1.0−2.8 Å. *R* window for CuO, 1.0−2.0 Å. Number of independent parameters for Cu K-edge fits, 9; number of adjusted parameters, 7. Number of independent parameters for the Se K-edge fits, 11−12; number of adjusted parameters, 9−10. In β-CuSCN, Cu is surrounded by 1 N at 1.93 Å and 3 S at 2.34 Å; S by 1 C at 1.70 Å and 3 Cu at 2.34 Å. In α-CuSCN, Cu is surrounded by 1 N at 1.93 Å and 3 S at 2.35−2.37 Å; S by 1 C at 1.70 Å and 3 Cu at 2.35 Å (*21, 33*).

phase mixture is also believed to be responsible for the vanishing of the third RDF peak for the sludge. Cu atoms are surrounded by a second C shell at 3.0−3.3 Å in thiocyanates (*21*; Table S2 in the Supporting Information). The nature of

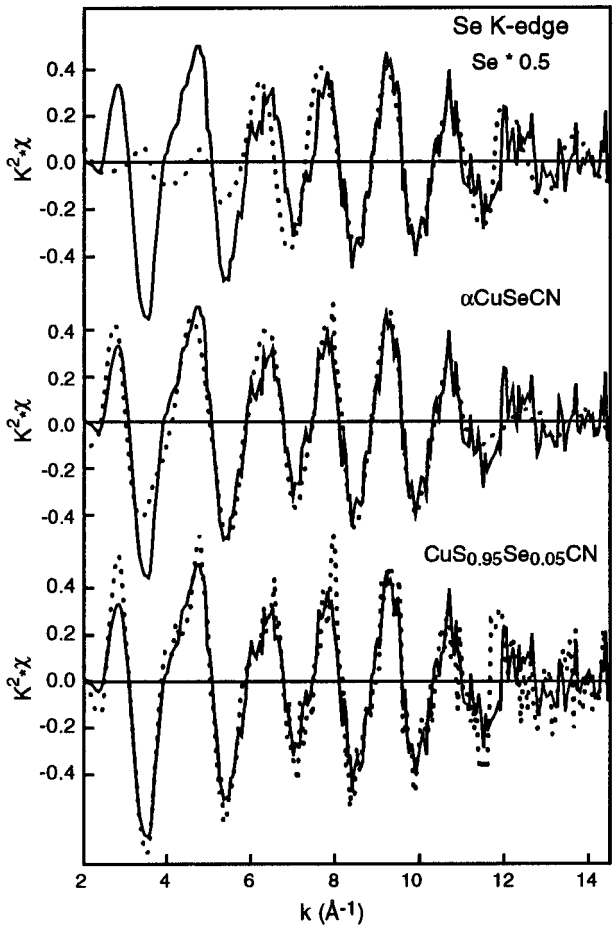

FIGURE 5. Comparison of k^2-weighted Se K-edge EXAFS spectra for the references (dotted lines) and the sludge sample (solid line).

next-nearest atomic neighbors in the oxyhydroxide/salt impurity is not known but, in any case, does not consist of carbon. This multiplicity of the various atomic environments around Cu atoms in the sludge sample beyond ~2.5 Å results in a sort of structural disorder that smears out the EXAFS signal and, consequently, RDF peaks beyond the first coordination shell.

Se K-edge. Se K-EXAFS spectrum for the sludge is superimposed on those of references in Figure 5. Its shape is similar to those of copper(I) cyanate samples and clearly different from elemental selenium. The frequencies and amplitude envelope of Se^0 and the sludge are markedly different at low *k*. This spectral comparison allows us to exclude the formation of native selenium, with a detection limit estimated to 8−10% and proves that the majority of selenium is located in a thiocyanate structure. The good spectral resemblance between elemental selenium and the sludge from 6−8 to 14.2 $Å^{-1}$ is noteworthy and indicates that both materials share some common structural features. The reason for this spectral likeness is given by the comparison of RDFs. Figure 4c shows the presence in both materials of an intense peak centered at ~2.05 Å, which corresponds to the first Se-Se pairing at the crystallographic distance of 2.36−2.37 Å in elemental Se (*29, 30*) and to the first Se-Cu metal shell contribution at ~2.4 Å in copper selenothiocyante structures (Table 2). Because of their close atomic number (*Z*) and similar distance from the central X-ray absorber (i.e., Se at the Se K-edge), Cu and Se atomic shells give a similar EXAFS signal. That this similarity is noticeable beyond 6−8 $Å^{-1}$ comes from the fact that the contribution of high *Z* elements predominates in this wavevector *k* range (*13*). On the other side, the high amplitude of the EXAFS signal for the sludge sample below 6 $Å^{-1}$ is a result of the presence of a low *Z* scatterer and specifically to C atoms belonging to cyanate (CN) groups. This C shell, which is located at ~1.7−1.9 Å in cyanate structures, gives rise to the RDFs peaks observed at 1.2−1.6 Å in Figure 4c.

In the sludge RDF, this Se-C peak is split, which indicates that Se−C distances are not unique and distributed over a certain range. Examination of the shape and position of this Se−C peak in cyanate samples of Figure 4c shows that the higher the Se content, the larger the average Se−C distance. Second RDFs peaks are clearly asymmetric, being broadened on their right side (see arrow in Figure 4c). This asymmetry indicates that Se−Cu distances are also incoherent. Accordingly, the structural disorder around Se atoms is not restricted to the first coordination shell but extends beyond. A parallel can be made between this disorder observed at the Angström scale and the width of diffraction peaks observed on XRD patterns (Figure 1). These two results are fully consistent and indicate that the Se for S substitution in the mineral lattice tends to lower the crystallinity by increasing the spread of distances in the cyanate framework.

Interatomic distances and number of atomic neighbors in each atomic shell were determined by a classical procedure, which consists of least squares fit inverse Fourier transforms (*13*). Se−C and Se−Cu RDF peaks were Fourier back-transformed together from the *R* to the wavevector *k* space because of the distance-related overlap of the various contributions. This mathematical operation yielded a partial EXAFS spectrum, which is the contribution to the whole EXAFS spectrum of the atomic shells that were selected by the windowing in the *R* space. Se−(C,Cu) partial EXAFS spectra are presented in Figure 6. As for whole EXAFS spectra, the contribution of low *Z* elements (i.e., C) are predominant in the low *k* range and that of high *Z* elements (i.e., Cu) are predominant in the high *k* range. Examination of Figure 6a shows that the differences noted in the RDFs for Se−C shells among the various samples give rise to different wave beat node patterns at 6−8 $Å^{-1}$. Likewise, the spread of Se−Cu distances noted in RDFs results in the presence of wave nodes at 10−12 $Å^{-1}$. Note that αCuSeCN has the strongest node, which is consistent with the higher asymmetry of its Se−Cu RDF peak (arrow in Figure 6a).

Based on the previous considerations, the spectral fitting should normally be conducted with a four-shell model: two Se−C shells and two Se−Cu shells. But in order to limit the number of free parameters in the fitting procedure, fitting trials were carried out with a three-shell model. The maximum number of independent parameters, N_{indep}, can be estimated from the formula $2\Delta k\Delta R/\pi$, where Δk is the *k*-range for the spectral fitting and ΔR is the width of the back-transform window. The number of free parameters was equal to 9−10 (Table 2), which is below N_{indep}, estimated to be 11−12 in this case. The omission of the fourth shell is also justified by the fact that for each sample three shells clearly predominate. The sludge sample has two marked Se−C pairs, and the long distance Cu shell can be neglected due to the fairly symmetric shape of its second RDF peak. The reverse trend is observed for cyanate references: the variation range of Se−Cu distances is larger, and Se−C distances seem to be relatively coherent.

Experimental and theoretical partial EXAFS spectra are shown in Figure 6b−d, and structural parameters are listed in Table 2. For the sludge sample, least-squares fitting resulted in ~0.3 C at 1.69 Å, ~0.9 C at 1.86 Å, and ~3 Cu at 2.42 Å. This Se−Cu distance is in good agreement with that determined at the Cu K-edge (2.41 Å). The Se−C distance of 1.86 Å corresponds to an increase of 0.16−0.17 Å relative to the S−C distance in α/βCuSCN, which is reasonable considering that Se^{2-} is 0.14 Å bigger than S^- (*22*). This Se−C distance is however slightly larger than that expected from ionic radii considerations, but fully agrees on a crystal chemical basis with the existence of few short bond lengths of 1.69 Å. The

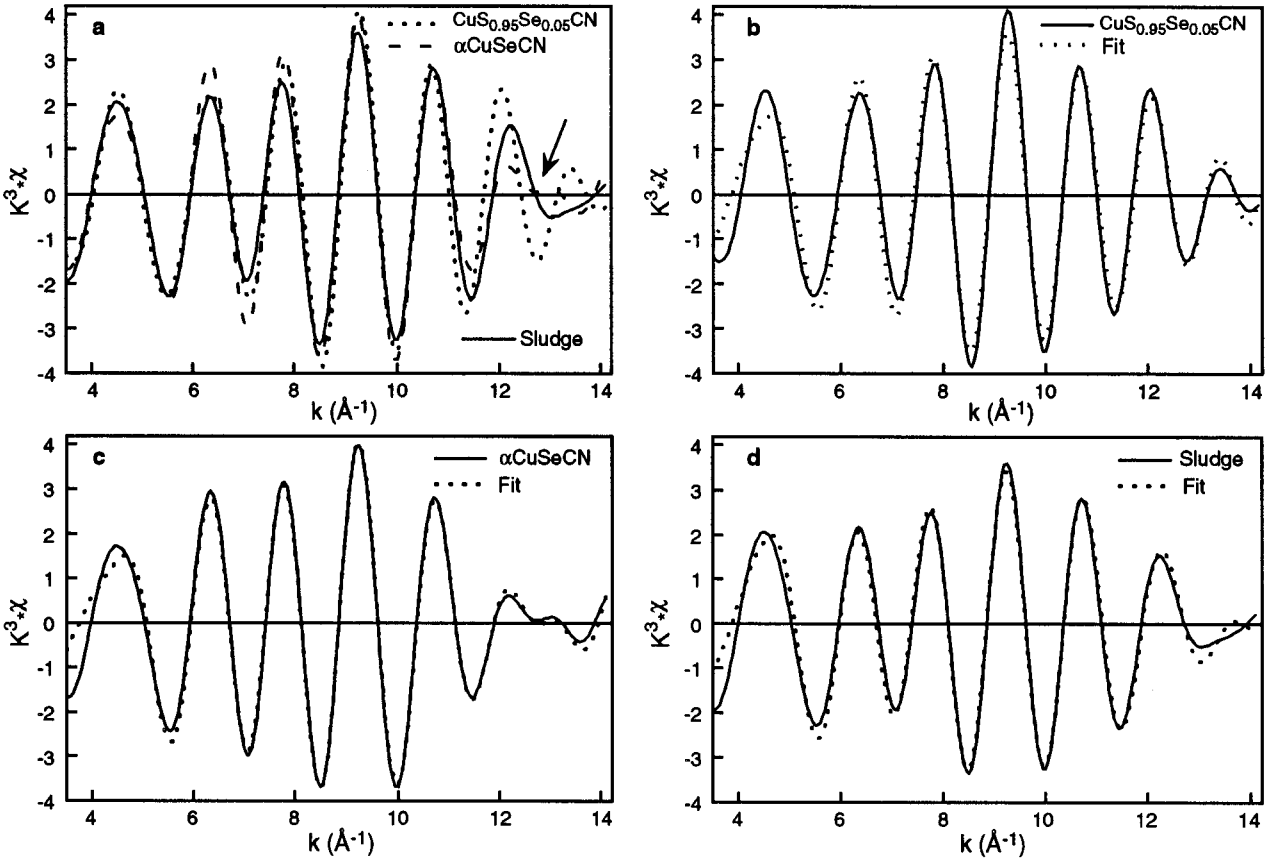

FIGURE 6. Fourier filtered Se−C and Se−Cu contributions to EXAFS for the sludge and references. (a) Comparison of experimental spectra. (b−d) Comparison of experimental (solid lines) and theoretical (dotted lines) spectra.

introduction of Se in the thiocyanate structure thus undergoes a distorsion of (S,Se) polyhedra. One may chiefly consider that the initial S−C distance is preserved in one-fourth (0.3/(0.3+0.9)) of the Se sites, the other three-fourths being larger. This increase of the Se−C and Se−Cu distances is consistent with the increase of unit-cell parameters determined by XRD.

Precipitation Process with Copper(II) Chloride. Results from IR, X-ray diffraction, and EXAFS spectrosocpy indicate that the precipitate generated by treating selenium-bearing wastewater with copper chloride at pH ~9−10 contains selenium in the form of αCu(S,Se)CN. At pH 1, the sole crystalline compound detected is native selenium metal. This study allows us to exclude the presence of Se^0 when the precipitation is carried out in basic media. In this process, copper is reduced from the cupric to cuprous state. Syntheses were performed in the laboratory to approach the nature of the reducing agent. Precipitates formed by copper(II) chloride/sulfate addition to KSeCN solutions consisted of $Cu(SeCN)_2$. More generally, all samples prepared by copper salt addition to selenocyanate solutions in the absence of thiosulfate or sulfurous acid yielded XRD spectra that resembled dithiocyanate copper. Thus, the reducing agent in the wastewater stream employed in the precipitation process likely consists of sodium salts of thiosulfate or sulfite. Accordingly, the removal of selenium is thought to be realized through the following reaction:

$$2CuCl_2 \cdot 2H_2O + 2x NaSeCN + (2 - 2x)NaSCN + 2Na_2S_2O_3 \rightarrow 2CuS_xSe_{1-x}CN + Na_2S_4O_6 + 4NaCl + 4H_2O$$

A slight excess of copper is added in the above precipitation step in order to improve the elimination rate of selenium from the wastewater. This excess of copper chloride accounts for the presence of unreduced cupric ions liganded to O, OH, or H_2O groups detected by Cu K-XANES and EXAFS measurements. Stated another way, the final Cu^+/Cu^{2+} ratio in the sludge depends on the relative concentration of added copper and of the reducing agents initially present in the wastewater.

To reduce the discharge of dissolved copper from the Se-free wastewater, caustic soda and/or sodium sulfide is added to the regenerant to precipitate the excess copper to below 1 mg/L:

$$CuCl_2 \cdot 2H_2O + 2NaOH \rightarrow Cu(OH)_2 + 2NaCl + 2H_2O$$

or

$$CuCl_2 \cdot 2H_2O + Na_2S \rightarrow CuS + 2NaCl + 2H_2O$$

Selenocyanate may alo be precipitated as poorly crystalline, elemental selenium with acids (*10*). Tests were carried out, but the selenium precipitation efficiency ranged from 25 to 75% over the pH range 2−4. Reduction of the pH of the refinery wastewater below 1 precipitated selenium quantitatively but generated significant, toxic hydrogen cyanide gas:

$$NaSeCN + HCl \rightarrow NaCl + HCN + Se$$

Efficiency of Se Removal with Various Metal Salts. The addition of excesses of silver(I) nitrate, tin(II) chloride, and copper(II) chloride to the refinery wastewater formed precipitates. For all these metal salts, the removal efficiency of selenocyanate was greater than 95%. By contrast, iron(II), iron(III), manganese(II), nickel(II), zinc(II), tin(IV), and alum had little effect on selenium removal, with an efficiency generally below 10%. The silver, tin, and gold precipitates have not been characterized. However, a tan precipitate resulting from tin(II) treatment of the water tested amorphous or poorly crystalline to X-ray diffraction. The pH of the water decreased dramatically upon treatment with tin(II) and tin(IV), but only tin (II) precipitated selenocyanate. The difference in the behavior of the tin species toward seleno-

cyanate is unexplained. Insoluble silver and gold selenocyanates have been documented (*10*).

The present study indicates that efficient removal of selenocyanate upon treatment of water containing reducing agents can be achieved with acid, silver(I), tin(II), and copper(II). Treatment of large volumes of water with relatively cheap acid to precipitate elemental selenium must advance with precaution because of solution corrosivity and hydrogen cyanide gas generation. Silver and tin salts are too expensive for treatment of wastewater. The most cost-effective precipitants for selenocyanate are copper(II) salts. Reducing agents may also be added to water to improve CuSeCN precipitation efficiency. Treatment of water with copper(II) salts must be carefully controlled to mitigate copper discharge from the Se-free wastewater. Secondary treatment of water with hydroxide or sulfide can reduce soluble copper levels to acceptable limits by the formation of copper hydroxides and covellite, respectively. Precipitated sludge from the water treatment process can be disposed by metal recyclers at a cost of approximately $25/t or benefically used as copper smelter feedstock ore.

Acknowledgments

We thank the staff of LURE for their technical support and Unocal Corporation management for permission to publish these results.

Supporting Information Available

Three tables (S1-S3) showing chemical analyses, X-ray diffraction, and structural data for thiocyanates and the sludge sample (3 pp) will appear following these pages in the microfilm edition of this volume of the journal. Photocopies of the Supporting Information from this paper or microfiche (105 × 148 mm, 24× reduction, negatives) may be obtained from Microforms Office, American Chemical Society, 1155 16th St. NW, Washington, DC 20036. Full bibliographic citation (journal, title of article, names of authors, inclusive pagination, volume number, and issue number) and prepayment, check or money order for $12.00 for photocopy ($14.00 foreign) or $12.00 for microfiche ($13.00 foreign), are required. Canadian residents should add 7% GST. Supporting Information is also available via the World Wide Web at URL http://www.chemcenter.org. Users should select Electronic Publications and then Environmental Science and Technology under Electronic Editions. Detailed instructions for using this service, along with a description of the file formats, are available at this site. To down-load the Supporting Information, enter the journal subscription number from your mailing label. For additional information on electronic access, send electronic mail to si-help@acs.org or phone (202)872-6333.

Literature Cited

(1) WSPA. *Selenium Removal Technology Study*; Western States Petroleum Association: Concord, CA, 1995.
(2) Haygarth, P. M. In *Selenium in the Environment*; Frankenberger, W. T., Benson, S., Eds.; Marcel Dekker, Inc.: New York, 1994; pp 1−27.
(3) Mayland, H. F. In *Selenium in the environment*; Frankenberger, W. T., Benson, S., Eds.; Marcel Dekker, Inc.: New York, 1994; pp 29−45.
(4) Pontius, F. W. *J. Am. Water Works Assoc.* **1995**, *2*, 48−57.
(5) Boegel, J. V.; Clifford, D. A. *U.S. EPA Report 600.2-86.031*; U.S. GPO: Washington, DC, 1986.
(6) Clifford, D. A. In *Water Quality and Treatment*; Pontius, F. W., Ed.; McGraw-Hill, Inc.: New York, 1990; pp 624−626.
(7) Lukasiewicz, R. J. Selenium speciation of process and discharge waters by IC-ICP-MS. Presented at Winter Conference on Plasma Spectrochemistry, San Diego, CA, January 1994.
(8) Altringer, P. B.; Lien, R. H.; Gardner, K. R. *Proc. SME-AIME Ann. Mg.—Gold'90* **1990**, 135−142.
(9) Gallup, D. L. In *Proceedings of the 69th Water Environment Federation Conference*, 1996, Dallas, TX; Water Environment Federation: Alexandria, VA, 1996; pp 447−453.
(10) Golub, A. M.; Skopenko, V. V. *Russ. Chem. Rev.* **1965**, *34*, 901−908.
(11) Soderback, E. *Acta Chem. Scand.* **1974**, *28*, 116−117.
(12) Krishnan, V.; Zingaro, R. A. In *Selenium*.; Zingaro, R. A., Cooper, W. C., Eds.; Van Nostrand Reinhold Co.: New York, 1974; pp 337−407.
(13) Teo, B. K. *EXAFS: Basic Principles and Data Analysis*; Inorganic Chemistry Concepts 9; Springer-Verlag: Berlin, 1986.
(14) Koningsberger, D. C.; Prins, R. *X-ray Absorption. Principles, Applications, Techniques of EXAFS, SEXAFS and XANES*; John Wiley & Sons: New York, 1988; 673 pp.
(15) Brown, G. E.; Calas, G.; Waychunas, G. A.; Petiau, J. In *Spectroscopic Methods in Mineralogy and Geology*; Hawthorne, F. C., Ed.; Mineralogical Society of America: Washington, DC, 1988; pp 430−512.
(16) Charlet, L.; Manceau, A. In *Environmental Particles*; Buffle, J., Van Leeuwen, H. P., Eds.; Lewis Publishers: Chelsea, MI, 1993; pp 117−164.
(17) Manceau, A.; Combes, J. M. *Phys. Chem. Miner.* **1988**, *15*, 283−295.
(18) Manceau, A. *Geochim. Cosmochim. Acta* **1995**, *59*, 3647−3653.
(19) McKale, A. G.; Veal, B. W.; Paulikas, A. P.; Chan, S. K.; Knapp, G. S. *J. Am. Chem. Soc.* **1988**, *110*, 3763−3768.
(20) Zingaro, R. A.; Cooper, W. C. *Selenium*; Van Nostrand Reinhold Company: New York, 1974.
(21) Smith, D. L.; Saunders, V. I. *Acta Crystallogr.* **1981**, *B37*, 1807−1812.
(22) Shannon, R. D.; Prewitt, C. T. *Acta Crystallogr.* **1969**, *B25*, 925−945.
(23) Wells, A. F. *Structural Inorganic Chemistry*; Oxford University Press: Oxford, 1984; 1382 pp.
(24) Bianconi, A. In *X-ray Absorption. Principles, Applications, Techniques of EXAFS, SEXAFS and XANES*; Koningsberger, D. C., Prins, R., Eds.; John Wiley: New York, 1988; pp 573−662.
(25) Garaj, J. *Chem. Zvesti* **1967**, *21*, 865.
(26) Porai-Koshits, M. A. *Zh. Strukt. Khim.* **1963**, *4*, 584.
(27) Brese, N. E.; O'Keeffe, M.; Ramakrishna, B. L.; von Dreele, R. B. *J. Solution State Chem.* **1990**, *89*, 184.
(28) Restori, R.; Schwarzenbach, D. *Acta Crystallogr.* **1986**, *B42*, 201.
(29) Cherin, P.; Unger, P. *Inorg. Chem.* **1967**, *6*, 1589.
(30) Keller, R.; Holzapfel, W. B.; Schulz, H. *Phys. Rev.* **1977**, *B16*, 4404.
(31) Pecile, C. *Inorg. Chem.* **1966**, *5*, 210−214.
(32) Morgan, H. W. *J. Inorg. Nucl. Chem.* **1961**, *16*, 367−368.
(33) Kabesova, M.; Dunaj-Jurco, M.; Serator, M.; Gazo, J. *Inorg. Chem.* **1976**, *17*, 161−165.

Received for review February 14, 1996. Revised manuscript received December 2, 1996. Accepted December 13, 1996.[⊗]

ES960138A

[⊗] Abstract published in *Advance ACS Abstracts*, February 15, 1997.